Importance of chamber gas pressure on processing of Al-based metallic glasses during melt spinning

H.W. Yang[1, 2*], R.C. Wang[2], X.G. Yuan[2], R.D. Li[2], J.Q. Wang[3], M.J. Tan[1]

[1]School of Mechanical and Aerospace Engineering, Nanyang Technological University, Singapore 639798, Singapore

[2]School of Materials Science and Engineering, Shenyang University of Technology, Shenyang 110870, China

[3]Shenyang National Laboratory for Materials Science, Institute of Metal Research, Chinese Academy of Sciences, Shenyang 110016, China

Abstract

The effect of chamber gas pressure on the amorphicity of $Al_{85}Ni_5Y_{10}$ alloy was studied for the melt spinning process. The amorphicity of as-quenched ribbons was characterized by X-ray diffraction (XRD) and differential scanning calorimetry (DSC). The chamber atmosphere pressure is crucial to the cooling rate of melt spinning. At high vacuum, at pressure less than 0.001 atm, fully crystalline fragments are obtained. Monolithic amorphous ribbons were only obtained at a gas pressure of 0.1 atm, 0.2 atm or higher. The extended contact length between ribbons and the copper wheel contributes to the high cooling rate of melt spinning in Al-based glass forming alloys; that is supported by images recorded by a high speed camera. Higher chamber pressure increases contact length between ribbons and the wheel, which is qualitatively

* To whom all correspondence should be addressed. Email: hwyang2000@hotmail.com

elucidated by Bernoulli's equation.

Keywords: Amorphicity; melt spinning; amorphous alloy; Bernoulli's equation; quenching rate

1. Introduction

Metallic glasses produced by rapid solidification techniques have enhanced mechanical, corrosion resistant and magnetic properties, which makes this class of materials attractive both for fundamental research and engineering applications [1-3]. Among the various rapid solidification techniques, melt-spinning is mostly used for Al, Fe-based amorphous ribbon production, due to its simplicity, efficiency and high cooling rate (up to 10^6 K/s) [4, 5]. In this process, a jet of liquid metal is ejected from a nozzle and impinges on the outer surface of a rotating copper wheel, where a thin layer is formed from a melt puddle and rapidly solidifies as a continuous ribbon. According to the nozzle-to-wheel distance (g), the melt-spinning technique is classified into chill block melt spinning (CBMS) and planar flow casting (PFC) [6, 7]. In the CBMS process, a free jet of liquid metal is ejected from a circular nozzle positioned at a sufficiently large (more than several millimeters) nozzle–wheel gap, while, in the PFC technique, a slit nozzle with a small nozzle-to-wheel distance (g<1 mm) is applied. In the latter process, the melt puddle is constrained between the nozzle lip and the wheel surface, the liquid puddle is more stable and tends to wet the wheel surface better than the free jet CBMS. Therefore, the ribbon obtained by PFC technique is much better than that prepared by the alternative free jet CBMS, which makes the PFC possible to

produce ribbons up to tens of centimeters in width.

The thermal, mechanical and physical properties of rapidly solidified metallic alloys have a strong dependence on its cooling rate, which in turn, depend on the melt spinning parameters [5, 6, 8, 9]. Therefore, thorough control of the spinning parameters for the rapid solidification process is important both from scientific and engineering points of view. The influence of melt spinning parameters on the structure and physical properties of rapidly quenched alloys has been discussed in various research and review papers [8-13]. Due to the improved thermal contact at the wheel-ribbon interface, the cooling rate increases with ejection pressures [11]. And increasing wheel speed or decreasing melt overheating leads to smaller ribbon thickness and enhanced heat transfer between ribbons and the chilling substrate, and hence also improves cooling rate [8, 14]. A higher cooling rate is obtained by filling He than Ar, which is attributed to the better conduction of the heat through gas layer between the melt pool and the quench wheel [12].

The effect of wheel surface speed, gas ejection overpressure, ambient atmosphere, nozzle-wheel gap, melt jet diameter, melt jet impingement angle and melt temperature on cooling rate, ribbon geometry and puddle formation has been well established [8-12, 14-21]. But, to date, the effect of chamber gas pressure on the ribbon production has not been established, except that Ray [22] stated that greater degree of amorphicity was achieved by melt spinning the molten alloy onto the chill wheel in a partial vacuum having an absolute pressure of less than about 5.5 cm Hg (0.072 atm). However, it was observed in this study that the chamber gas pressure has a very strong, but contrary

effect on glass formation and cooling rate. In this paper, the effect of chamber gas pressure on glass formation and cooling rate of an Al-based alloy is presented, and an elucidation is proposed based on Bernoulli's equation.

2. Experimental Details

$Al_{85}Ni_5Y_{10}$ (atomic percentage) ingot was prepared by arc melting pure Al, Ni and Y elements in an Ar protected atmosphere, and re-melted 4~5 times to assure a composition homogeneity. Melt spinning was performed at the PFC mode using a laboratory scale single roller melt-spinning device operating in a purified Ar atmosphere or vacuum. The processing variables (wheel speed, gas ejection overpressure, nozzle-wheel gap or melt temperature) except chamber gas pressure were fixed to constant values. The slit of the ejection nozzles was fixed to be 0.7 by 2.5 mm throughout the study. The wheel speed ω was set to 31 m/s and the melt temperature was 1100 ± 10 ^{o}C (monitored by a two-color infrared pyrometer). The gas ejection overpressure was constant at 0.2 atm. The chamber pressure of filled Ar was set to be 0.2, 0.1, 0.01 and less than 0.001 atm, respectively. The amorphicity of the as-quenched ribbons was characterized by X-ray diffractometry with Cu K_α-radiation (Rigaku D/max 2400) and DSC (Perkin Elmer DSC-7) at a constant heating rate of 40 K/min. A high speed camera was engaged to record the melt spinning process at a frame rate of 2000 fps.

3. Results and discussion

The obtained ribbons are about 20 μm in thickness and 3 mm in width. The ribbon thickness is independent of the chamber gas pressure. Fig. 1 shows the XRD patterns of

the as-quenched ribbons spun at chamber pressure of <0.001, 0.01, 0.1 and 0.2 atm, respectively. The XRD patterns spun at 0.1 and 0.2 atm have no sharp diffraction peaks of crystals could be observed. However, sharp peaks corresponding to Al crystalline diffraction are overlapped on the broad amorphous diffraction peak for the sample spun as 0.01 atm. The samples spun at a pressure less than 0.001 atm are fragmentary and fully crystalline, diffraction peaks of Al and other intermetallics are obviously observed.

DSC scanning was carried out on the as-quenched samples to characterize their thermal property. The DSC curves of the samples spun at 0.01, 0.1 and 0.2 atm are shown in Fig. 2. A glass transition signal is shown for the samples spun at a gas pressure of 0.1 or 0.2 atm, and then a series of exothermic peaks corresponding to crystallization. But for the samples spun at 0.01 atm, no glass transition could be observed, and the first crystallization peak corresponding to nano-Al precipitation vanishes. The glass transition temperature (T_g), onset crystallization temperature (T_x), enthalpy of crystallization (ΔH) and the structural state are summarized in Table 1.

It is well known that the principle of glass formation is to avoid crystallization during solidification. If the cooling rate is high enough, the nucleation of crystals is suppressed, the liquid metal transforms into glassy state directly by glass transition; or else, nucleation during the cooling process is possible, but the growth of the nuclei is limited in some marginal alloys[23]. For Al-based glass forming system, if the cooling rate is not high enough, the ribbons will be partially amorphous. At much lower cooling rate, fully crystalline samples will be produced.

From the above results presented, it is obvious that the amorphicity of $Al_{85}Ni_5Y_{10}$ alloy has remarkable dependence on the filled atmosphere pressure in the chamber. One may expect that some heat of the molten alloy was extracted by the Ar atmosphere by convection and radiation during the "free-flight period" where the ribbon separates from the wheel[24], which caused the different cooling rate; therefore high gas pressure could extract more heat to cool the liquid metal. But, as it is well-known that the heat capacity of Ar gas is very small (λ=0.01620 W/(m.K)), the convection of Ar gas is therefore not a sufficient heat transfer process. There must be some other factors or reasons to affect the cooling rate of melt spinning.Since the convection of inert gas is insufficient for the high cooling rate to form metallic glasses, the high cooling rate of melt spinning can only be obtained by a rapid heat transfer from the sample directly to the copper wheel. The cooling rate of melt spinning R_c is normally 10^5~10^6 K/s. The temperature of the melt alloy used in the present experiments was 1100 ^oC, and that of the obtained ribbons was about 50 ^oC, so the temperature difference ΔT for solidification is about 1050 K. The time needed for cooling down liquid metal into solid ribbons ($\Delta t = \Delta T/R_c$) should thus be between10^{-3}~10^{-2} seconds, and the residential length of the ribbon over the quenching wheel needed for accomplishing liquid-to-glass transition ($\Delta l = v * \Delta t$, here v is wheel speed of 31 m/s) should be between 0.03~0.3 meters. Looking more closely, it was observed that the ribbons departed from the wheel surface at different angles, and this depended strongly on the chamber gas pressure. When the atmosphere pressure was lower than 0.001 atm, the fragmentary ribbons were detached from the copper wheel at a direction almost perpendicular to the ejection direction, and the contact length

between the ribbon and the copper wheel was merely about 10 mm, as shown in Fig. 3(a). The samples coming off the wheel were still glowing, which indicates that the temperature of the sample off the copper wheel was still quite high, and the sample had not solidified after such a short contact with the copper wheel. The subsequent cooling process must consequently be completed in the inert gas atmosphere. As mentioned earlier, the limited heat capacity of the inert gas does not provide a high enough cooling rate to accomplish a glass transition, therefore, samples spun at such a low pressure remained crystalline. However, for the gas pressure of 0.01, 0.1 or 0.2 atm, the contact length of ribbon and wheel was extremely extended. The residential length of the ribbon on the wheel surface consequently increases to about 40, 80 and 120 mm corresponding to gas pressure of 0.01, 0.1 or 0.2 atm, respectively, which is shown in Fig. 3 (b), (c) and (d). (Corresponding high speed camera videos are also included as supplementary materials.) At the detaching point, the samples have been cooled down, solidified and fully or partially transformed into glassy ribbons. The extended contact with the copper wheel thereby accounts for the enhanced cooling rate of samples during melt spinning process. The heat of the melt is mostly transferred to the copper wheel, and therefore a high cooling rate aiding glass formation is obtained.

There must be some intrinsic factors influencing the contact length of the ribbon and the copper wheel. The gas flowing velocity on the wheel surface decreases sharply with distance, as schematically illustrated in Fig. 4; therefore, the gas velocity on the contact side of the ribbon is much higher than that on the free side. From Bernoulli's

equation, the total pressure ($P_t = P_s + P_d$) of fluid is the sum of the static pressure (P_s) and the dynamic pressure ($P_d = \rho V^2/2$), which keeps constant in a fluid system. That is

$$P_{s1} + \rho V_1^2/2 = P_{s2} + \rho V_2^2/2$$

In the above equations, ρ is the density of the fluid, V is the flowing velocity. From the equation, the static pressure P_s decreases with the increase of fluid velocity. Consequently, the static gas pressure P_s on the ribbon's free side is larger than that on the contact side. The ribbon is forced to stick to the rolling wheel surface. The velocity difference between the wheel side and the free side is larger at high chamber gas pressure than that at low gas pressure. The contact length of the ribbon on the copper wheel surface is therefore lengthened with filled gas, and also heat is more rapidly transferred from the ribbon to the copper wheel. Hence, high chamber gas pressure contributes to the cooling rate for melt spinning. The phenomena of amorphicity depending on gas pressure could be qualitatively elucidated by Bernoulli's equation.

The density and viscosity of the melts might be considered to have strong influence on the residential length of the ribbons. Some other alloy like an Fe-based alloy GFA of 2-3 mm was spun for comparison, where the alloys could not form a glass at very high vacuum circumstances either. Higher density of alloy provides more gravity that makes the ribbon stick to the wheel; meanwhile higher density also introduces more centrifugal force that pull the ribbon off the rotating wheel. Both the centrifugal force and gravity are proportional to the density, and they offset each other, therefore the density of alloys has no influence on the residential length. Viscosity is another factor that may influence the contact length between the ribbon and the wheel. The viscosity of the melt decreases

with its temperature. Al-based melts with various temperatures were spun at high vacuum and partial atmosphere. No obvious difference in contact length was observed for the melt at temperature range of 950^{o}C-1250^{o}C.

One may also expect that much higher chamber pressure (like 1 atm) should provide higher cooling rate that 0.2 atm. In the present study, the 0.2 atm is high enough for the melt to be transformed into glass. The liquid alloy has been cooled down to temperature lower than the glass transition temperature at 0.2 atm with a contact length of ~120 mm, even if the higher pressure (like 1 atm) could extend the ribbon residential length, after the transformation is accomplished it does not improve liquid-to-glass transition any more.

Liebermann studied surface dynamics of melt spinning, and observed that the sticking distance of ribbon on the wheel increases with wheel revolution[25]. In the present study, the contact length has tiny fluctuations throughout the whole run due to atmospheric turbulence. But no noticeable surface dynamic effect was observed, and the contact length has no obvious change during the whole melt spinning run (As shown by the high speed camera videos in the supplement materials). The paper mentioned that the ribbon-substrate sticking distance increases much faster with revolutions at higher wheel speed when the other parameters are kept constant [25]. The author attributed this to the higher rate of wheel track heating at higher linear velocities. However if the other parameters keep unchanged, the track heating rate should also be constant at equivalent revolutions. According to present study, greater gas flow speed difference between the contact side and the free side of the ribbon is introduced at higher wheel speeds, which

provides higher force pushing the ribbon to stick to the rotating wheel. The results presented in reference [25] also support the point in the present study.

4. Conclusions

The chamber atmosphere pressure has a strong influence on the cooling rate of melt spinning process. Fully amorphous ribbons are fabricated at gas pressure of 0.1 and 0.2 atm, but only partially amorphous structure is obtained at a gas pressure of 0.01 atm for $Al_{85}Ni_5Y_{10}$ alloy. If the chamber pressure is lower than 0.001 atm, crystalline fragments are produced by melt spinning. Higher chamber pressure increases contact length between ribbons and the wheel, which accounts for the high cooling rate of melt spinning to form metallic glasses.

Acknowledgements

This work was financially supported by ASTAR SERC (Grant No. 092 137 0018), National Natural Science Foundation of China (Grant No. 50874075) and Project of Shenyang Bureau of Science and Technological Development (Grant No. 1091177-1-00).

References

[1] S.J. Pang, T. Zhang, K. Asami and A. Inoue, Acta Mater. 50 (2002) p. 489.

[2] J.M. Park, Y.C. Kim, W.T. Kim and D.H. Kim, Mater. Trans. 45 (2004) p. 595.

[3] K. Amiya, A. Urata, N. Nishiyama and A. Inoue, Mater. Trans. 45 (2004) p. 1214.

[4] A. Inoue, K. Ohtera, A.P. Tsai and T. Masumoto, Jpn. J. Appl. Phys. 2 27 (1988) p. L280.

[5] I. Bakonyi, F. Mehner, M. Rapp, A. Cziraki, H. Kronmuller and R. Kirchheim, Z. Metallk. 86 (1995) p. 619.

[6] S. Budurov, M. Lazarova, G. Stephani and H. Fiedler, Mat. Sci. Eng. A 133 (1991) p. 448.

[7] M.C. Narasimban, U.S. Patent No. 4212343 (1980).

[8] A. Revesz, A. Concustell, L.K. Varga, S. Surinach and M.D. Baro, Mat. Sci. Eng. A 375-77 (2004) p. 776.

[9] J.K. Lee, D.H. Bae, W.T. Kim and D.H. Kim, Mat. Sci. Eng. A 375-77 (2004) p. 332.

[10] O.V. Tolochko and N.O. Gonchukova, Glass Phys. Chem. 30 (2004) p. 532.

[11] Y. Sato, K. Fukutani and M. Yamate, J. Jpn. Inst. Met. 57 (1993) p. 1204.

[12] M.J. Kramer, Y. Tang, K.W. Dennis and R.W. McCallum, Mater. Res. Soc. Symp. Proc. 577 (1999) p. 57.

[13] H.A. Davies, Rapidly Quenched Met., Proc. Int. Conf., 3rd (1978) p. 1.

[14] V.I. Tkatch, A.I. Limanovskii, S.N. Denisenko and S.G. Rassolov, Mat. Sci. Eng. A 323 (2002) p. 91.

[15] H.H. Liebermann, Mater. Sci. Eng. 43 (1980) p. 203.

[16] H. Hillmann and H.R. Hilzinger, Rapidly Quenched Met., Proc. Int. Conf., 3rd 1 (1978) p. 22.

[17] L. Katgerman and P.J. Van den Brink, Proc. Int. Conf. Rapidly Quenched Met., 4th 1 (1982) p. 61.

[18] P.H. Shingu, K. Kobayashi, R. Suzuki and T. K., Proc. Int. Conf. Rapidly Quenched Met., 4th 1 (1982) p. 57.

[19] G. Li and B.G. Thomas, in: J.K. Brimacombe and I.V. Samarasekera (Eds.) Proceedings of the International Symposium on Near-Net-Shape Casting in the Minimills, Vancouver, 1995, pp. 373.

[20] H.H. Liebermann, Rapidly Quenched Met., Proc. Int. Conf., 3rd 1 (1978) p. 34.

[21] H.H. Liebermann, J. Appl. Phys. 50 (1979) p. 6773.

[22] R. Ray, US Patent No. 4067732 (1978).

[23] J.H. Perepezko, R.J. Hebert and W.S. Tong, Intermetallics 10 (2002) p. 1079.

[24] M.J. Kramer, H. Mecco, K.W. Dennis, E. Vargonova, R.W. McCallum and R.E. Napolitano, J. Non-Cryst. Solids 353 (2007) p. 3633.

[25] H.H. Liebermann, Metall. Trans. B 15 (1984) p. 155.

Table 1, Glass transition temperature (T_g), crystallization temperature (T_x), enthalpy released by crystallization (ΔH) and state of the produced samples spun at a filled gas pressure of 0.001, 0.01, 0.1 and 0.2 atm.

Gas	T_g (^{o}C)	T_x (^{o}C)	ΔH (J/g)	State of the products
0.2	260 ±0.5	285 ±0.5	157 ±2	Fully amorphous
0.1	255 ±0.5	277 ±0.5	153 ±2	Fully amorphous
0.01		365 ±0.5	76 ±2	Partially amorphous
<0.001				Fully crystalline

Figure captions:

Fig. 1 XRD patterns of the samples spun at wheel speed of 31m/s at chamber gas pressure of <0.001, 0.01, 0.1 and 0.2 atm, respectively.

Fig. 2 DSC profiles for the samples spun at chamber pressure of 0.01, 0.1 and 0.2 atm at a heating rate of 40 ^{o}C/min, T_g and T_x shows the glass transition and the onset crystallization temperatures, respectively.

Fig. 3 Images taken by a high speed camera indicating residential lengths of ribbons on the chill wheel at chamber gas pressures of (a) less than 0.001 atm, (b) 0.01 atm, (c) 0.1 atm and (d) 0.2 atm, the white arrows indicate the detaching points the ribbons or fragments from the chill wheel.

Fig. 4 Schematic illustration of the velocity distribution of the flowing gas over the wheel surface.

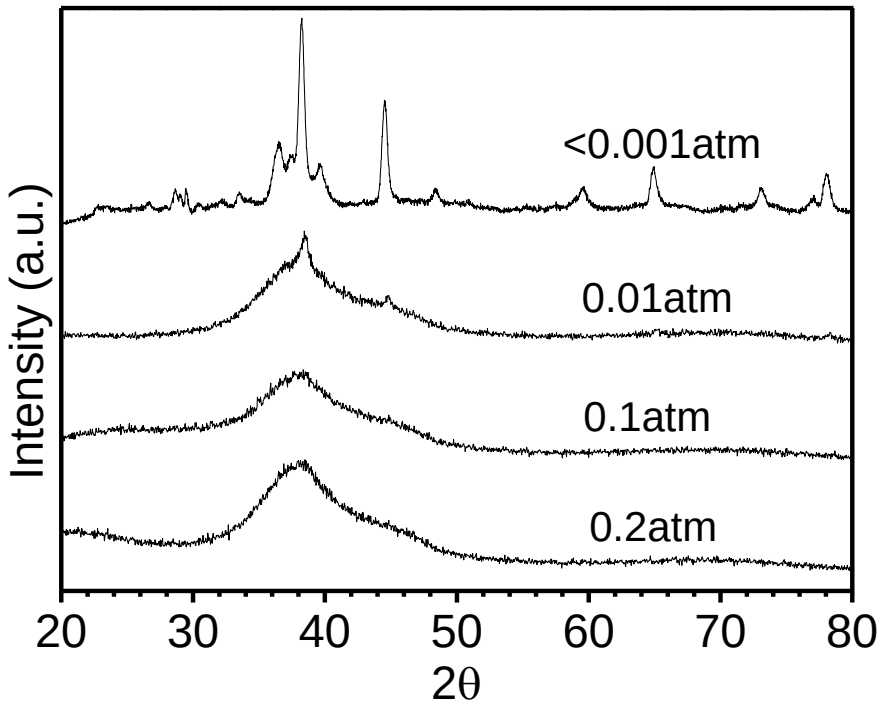
<0.001atm
0.01atm
0.1atm
0.2atm
Intensity (a.u.)
20
30
40
50
60
70
80
2θ

Figure 1

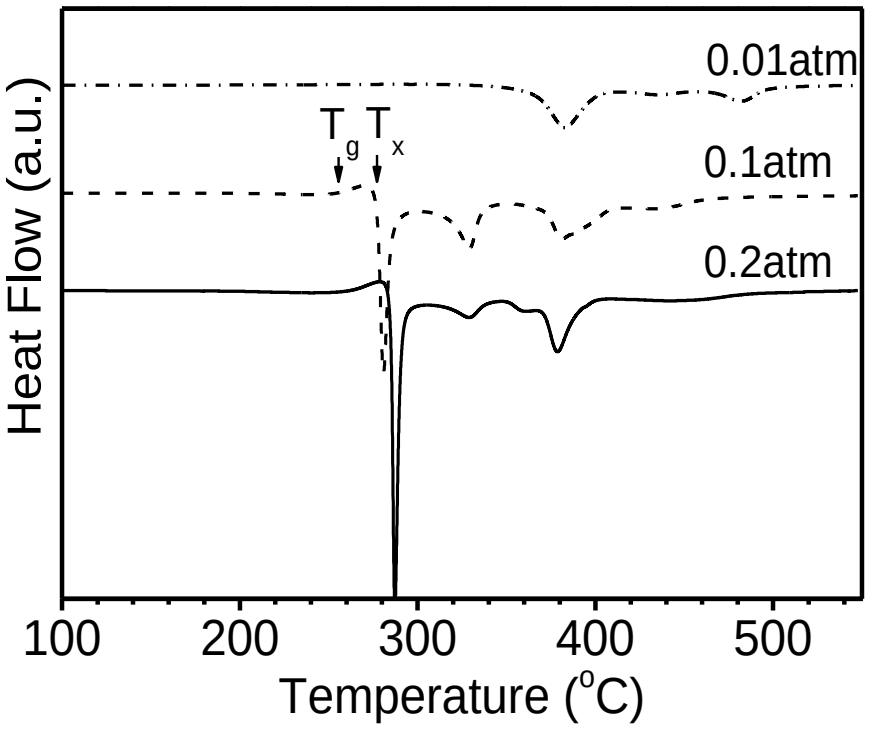
0.01atm
0.1atm
0.2atm
T g
T x
Heat Flow (a.u.)
100
200
300
400
500
Temperature (°C)

Figure 2

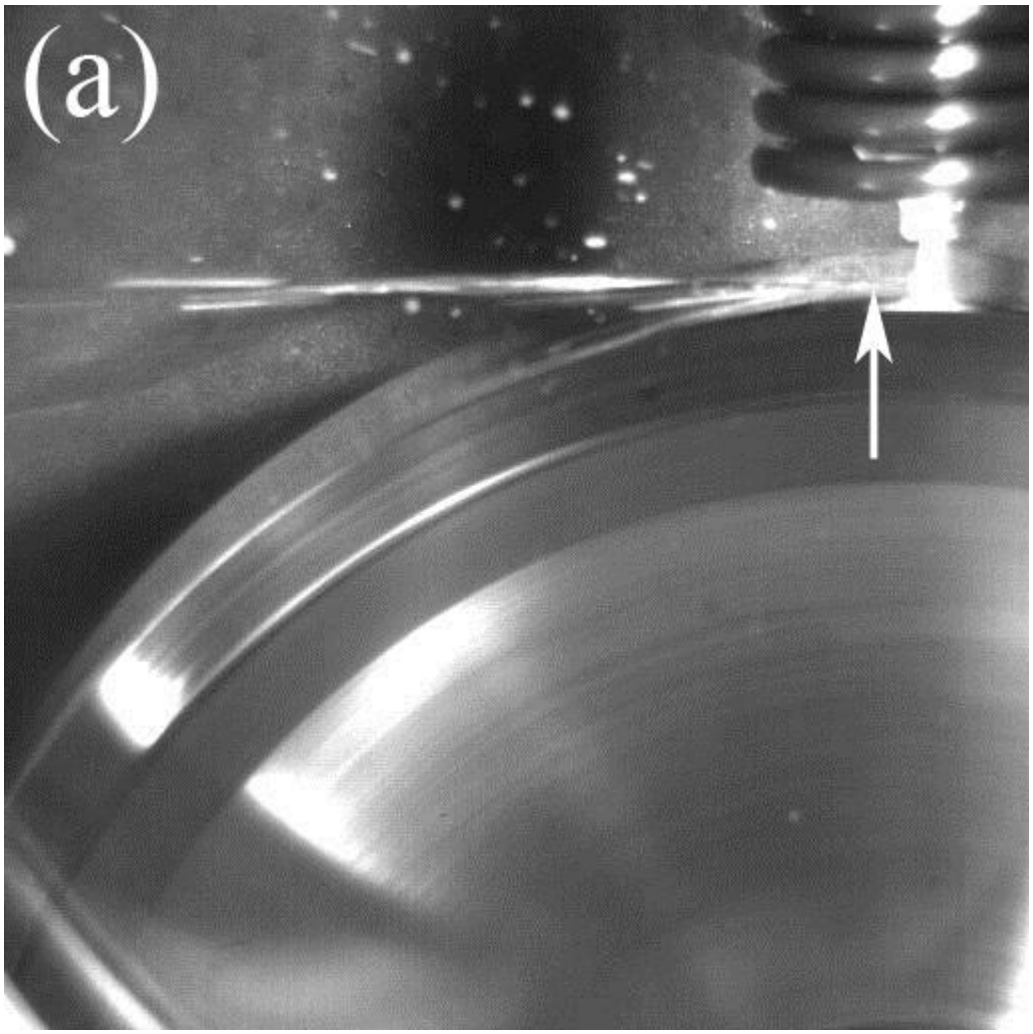

Figure 3(a)

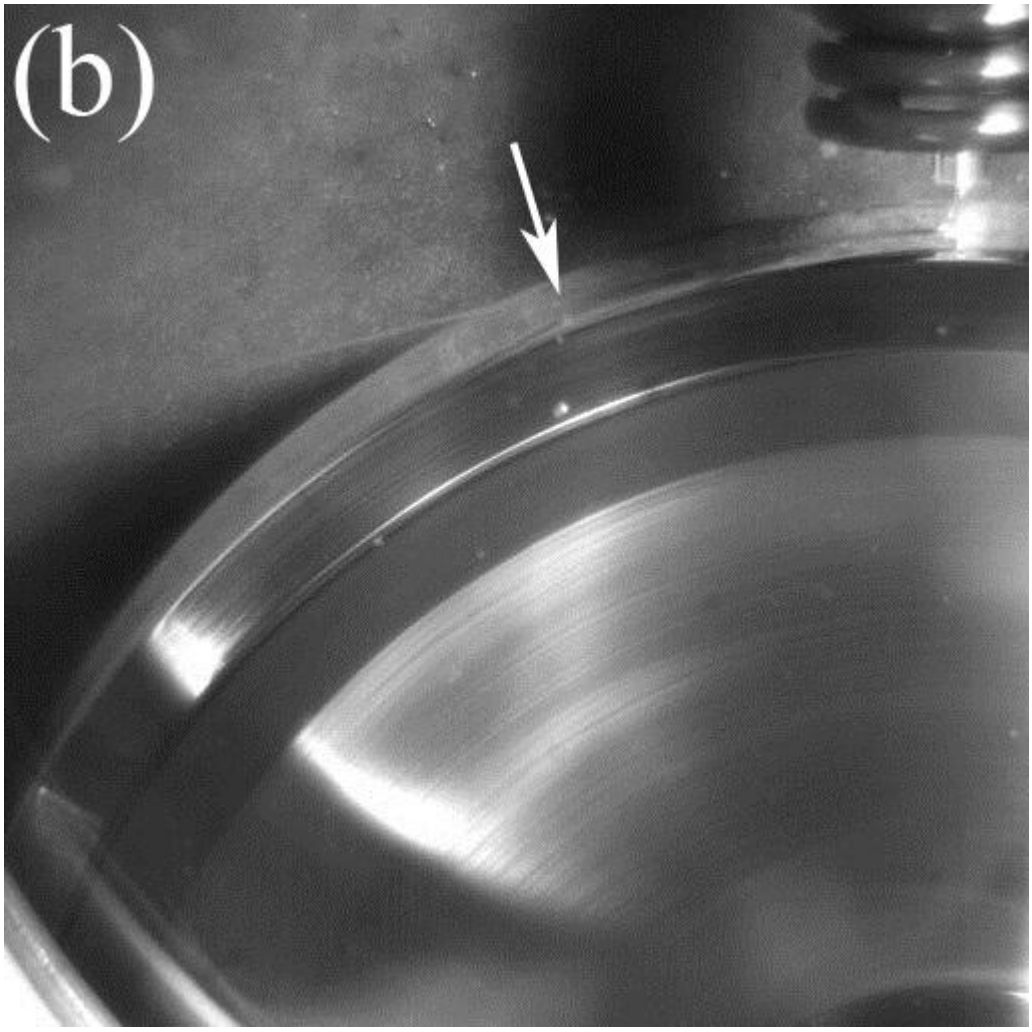

Figure 3(b)

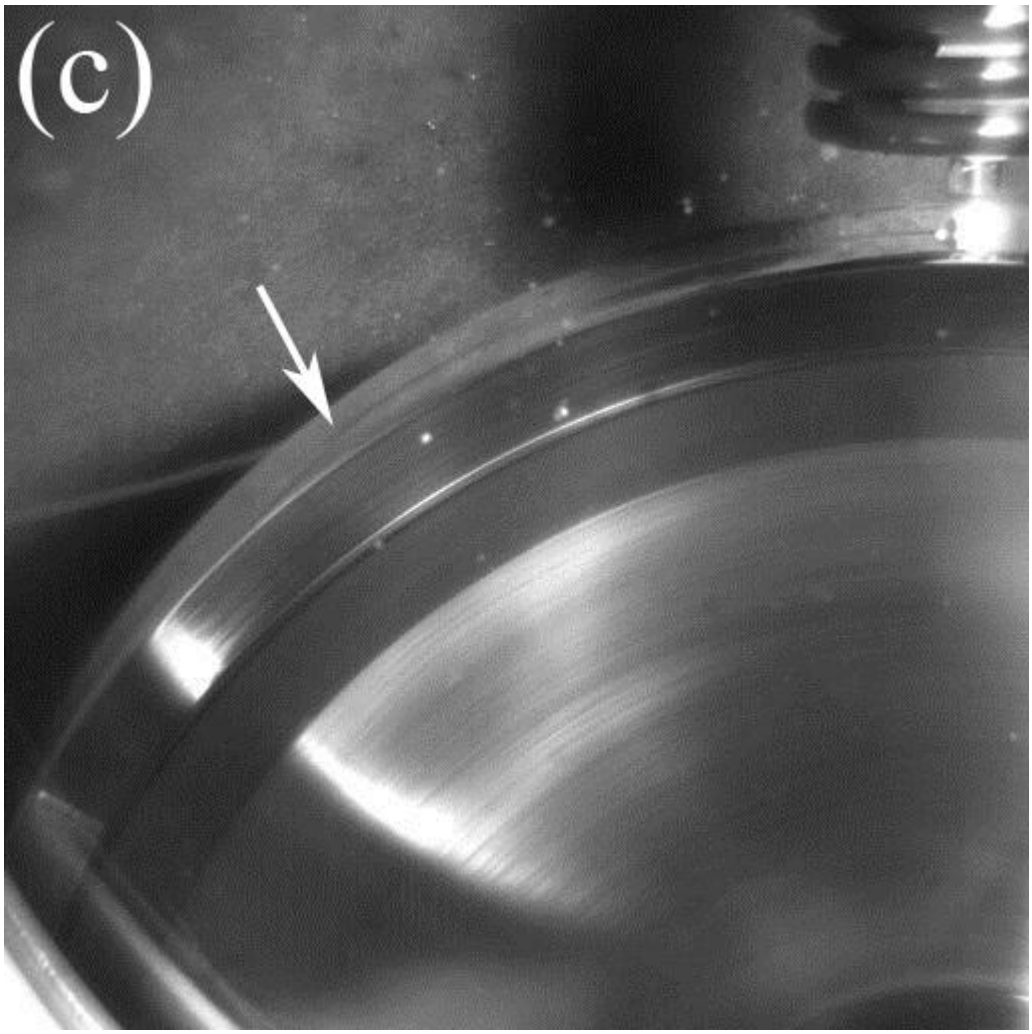

Figure 3(c)

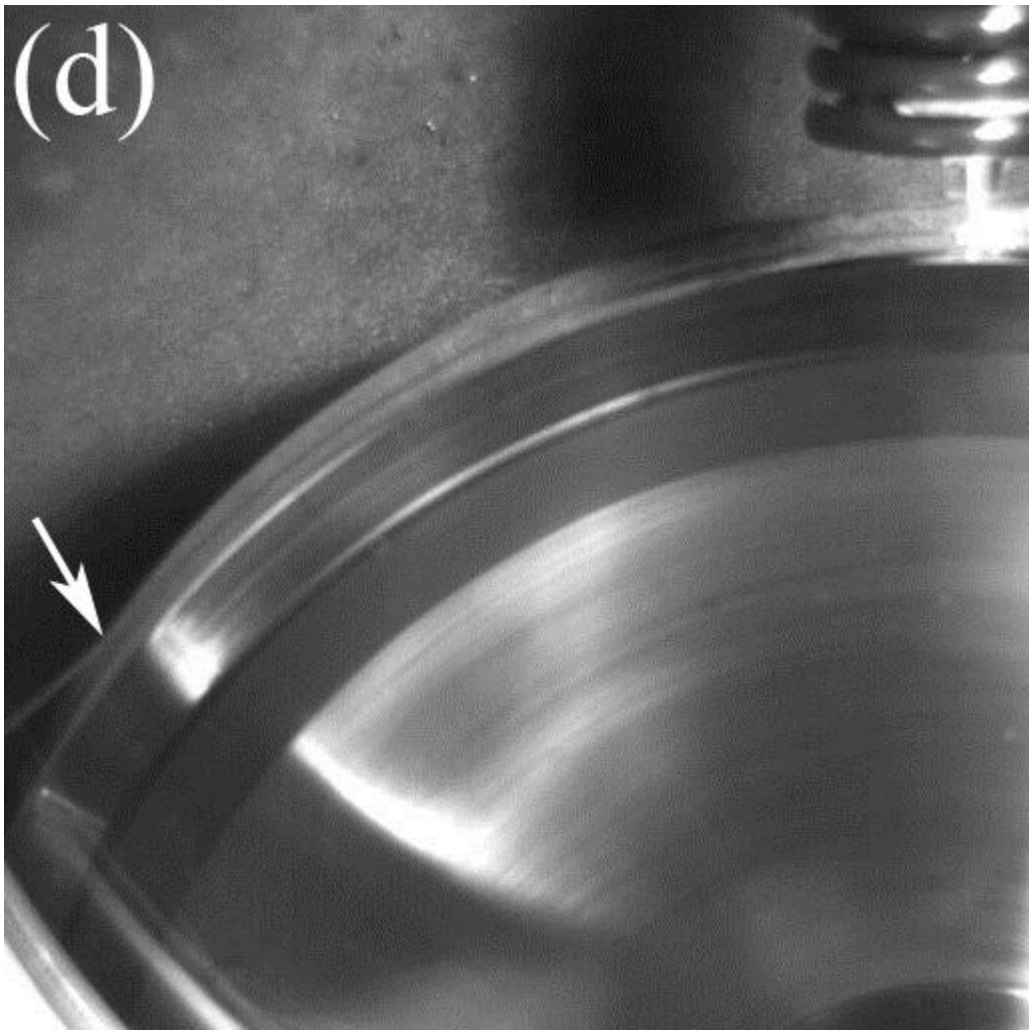

Figure 3(d)

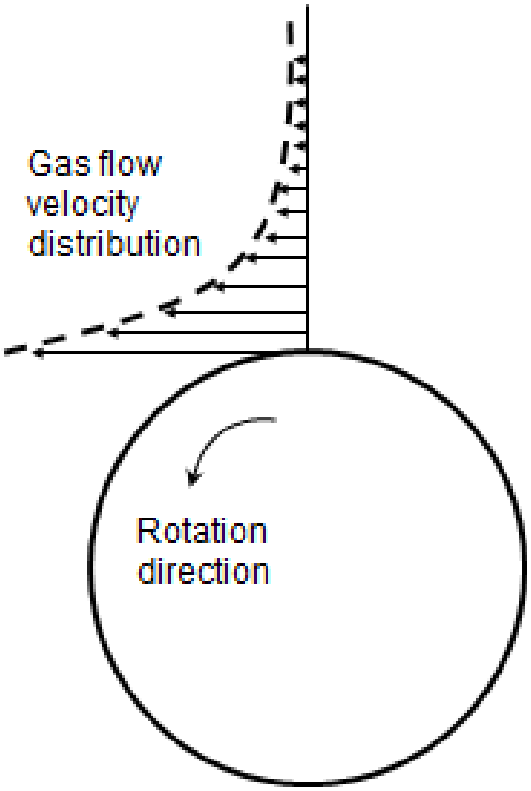

Figure 4